Astron. Astrophys. 323, 349–356 (1997)

ASTRONOMY
AND
ASTROPHYSICS

The distribution of ionized gas in early-type galaxies

III. M/L determinations based on triaxial models⋆

A. Pizzella[1], P. Amico[2], F. Bertola[1], L.M. Buson[3], I.J. Danziger[2,4], H. Dejonghe[5], E.M. Sadler[6], R.P. Saglia[7], P.T. de Zeeuw[8], and W.W. Zeilinger[9]

[1] Dipartimento di Astronomia, Università di Padova, Italy
[2] European Southern Observatory, Garching bei München, Germany
[3] Osservatorio Astronomico, Capodimonte, Napoli, Italy
[4] Osservatorio Astronomico, Trieste, Italy
[5] Sterrenkundig Observatorium, Universiteit Gent, Belgium
[6] Astrophysics Department, School of Physics, Univ. of Sydney, Australia
[7] Universitäts-Sternwarte München, Germany
[8] Sterrewacht Leiden, The Netherlands
[9] Institut für Astronomie, Universität Wien, Austria

Received 20 May 1996 / Accepted 2 January 1997

Abstract. The velocity fields of ionized gas disks in four elliptical galaxies have been exploited to derive the mass-to-light ratios as function of radial distance. For each galaxy, namely NGC 1453, NGC 2974, NGC 5077 and NGC 7097, we derive a set of intrinsic shapes of the stellar component and viewing angles that are consistent with the observed ellipticities and orientation of the isophotes. A least-squares fit to the observed velocity field gives the set of parameters defining the potential that best reproduces the kinematics of the ionized gas disk as well as the mass density and light density radial profiles. For three galaxies a satisfactory model is found. The M/L ratio does change within individual galaxies, though not showing any systematic increase with radius and has a mean value of about $5 M_{\odot}/L_{B\odot}$ out to $\sim 1 R_e$.

Key words: galaxies: elliptical and lenticular, cD – galaxies: ISM – galaxies: structure – galaxies: kinematics and dynamics

1. Introduction

This is the third in a series of papers on the properties of elliptical galaxies with ionized gas disks that have been produced by the ESO Key Programme "A search for dark matter in elliptical galaxies" (Bertin et al. 1989). In Paper I (Buson et al. 1993) the H_α imaging for 15 galaxies known to have emission lines was presented and discussed. Follow up spectroscopic observations, which map the velocity field of the ionized gas, were made for six objects with regular gas morphology, and were presented in Paper II (Zeilinger et al. 1996). In this third paper we compare these datasets, three velocity fields from Paper II and one, NGC 5077, from Bertola et al. (1991, hereafter B91), with models for the non–circular velocity fields of cold gas in triaxial potentials. The models allow us to correlate the parameters related to the intrinsic shape of the galaxy with the observed ellipticity values and the position angle of the stellar major axis. The fits to the velocity field and to the luminosity profile give the mass and light density profiles respectively and hence the radial mass-to-light profile. The method is similar to that developed by de Zeeuw and Franx (1989, hereafter ZF) and applied by B91 to NGC 5077. Here we consider models with cusped central density profiles. The extension of the ionized gas disks is typically of the order of one effective radius, R_e, or less. Our study is therefore limited to the inner regions of the galaxies.

2. Mass models

B91 used the family of separable triaxial models with constant density cores described by ZF to reproduce the ionized gas velocity field of NGC 5077 with a constant M/L model. Hubble Space Telescope observations indicate that elliptical galaxies generally have cusped central surface brightness profiles (Crane et al. 1993; Jaffe et al. 1994). Accordingly, we adopt the same approach as in B91, but we use a family of non-rotating triaxial mass models with a central density cusp. They are triaxial generalization of the so-called γ-models (e.g., Carollo 1993;

Send offprint requests to: Alessandro Pizzella, Dipartimento di Astronomia, Vicolo dell'Osservatorio 5, I-35122 Padova, Italy (pizzella@astrpd.pd.astro.it)

⋆ Based on observations collected at the European Southern Observatory, La Silla (Chile).

Dehnen 1993; Tremaine et al.1994) introduced and described in detail by de Zeeuw & Carollo (1996, hereafter ZC). These models allow for variations of ellipticity and position angle of the major axis of the isophotes with radius.

The mass models introduced by ZC are based on the spherical γ-models with density profile:

$$\rho(r) = \frac{(3-\gamma)\mathscr{M}_{\mathscr{T}} r_0}{4\pi} \frac{1}{r^{-\gamma}(r+r_0)^{4-\gamma}}. \quad (1)$$

This spherical density, and its associated gravitational potential, are functions of three parameters: $\gamma, \mathscr{M}_{\mathscr{T}}, r_0$. The first of these, γ ($0 \leq \gamma < 2$), measures the "cuspiness" of the central density profile which diverges as $1/r^{\gamma}$. For high values of γ we have a steep central profile while the case $\gamma = 0$ corresponds to the model with finite central density and a central density gradient intermediate between the King and Hubble profiles, similar to the separable models described by ZF, and applied by B91. $\mathscr{M}_{\mathscr{T}}$ is the total model-mass of the galaxy, and r_0 is a scale-length, which is related to R_e (Dehnen 1993).

The models are made triaxial by adding two low order spherical harmonics terms to the potential of the spherical γ models, with appropriately chosen radial functions, given in Eq. (2.5) of ZC. This introduces four free parameters in addition to $\gamma, \mathscr{M}_{\mathscr{T}}$ and r_0, which can be chosen as the intrinsic axis ratios p_0, q_0, p_∞, q_∞ of the triaxial surfaces of constant density at small and large radii, respectively.

A stable configuration of cold gas in a nonrotating triaxial galaxy can only be a ring or a disk in one of two principal planes, either perpendicular to the long axis of the figure or perpendicular to the short axis (Tohline, Simonson & Caldwell, 1982; Merritt & de Zeeuw, 1983). We use the convention that the Z axis is always perpendicular to the gaseous disk, and that the X axis is longer than the Y axis. From these definitions it follows that we have two distinct cases: when $1 \geq p \geq q \geq 0$ the gas is perpendicular to the short axis, and when $q \geq 1 \geq p \geq 0$ the gas is perpendicular to the long axis. The seven parameters $\gamma, \mathscr{M}_{\mathscr{T}}, r_0, p_o, q_o, p_\infty, q_\infty$ allow us to determine the 3-dimensional density distribution and the orbital velocities on either of the two relevant principal planes. We use the properties of the velocity field as derived by ZC by means of the first order epicyclic approximation. The projected surface density and projected velocity field, which are the observable quantities, are derived once we know the three viewing angles θ and ϕ, defined as the standard spherical coordinates of the line–of–sight in the galaxy coordinate system, and χ, the position angle of the projected Z axis, measured eastwards of North. The gas moves on closed orbits whose properties are fully determined by the model. The orbits become circular at large radii ($r >> r_0$) whereas the ellipticity ϵ_R reaches a maximum value for small radii ($r << r_0$) which is the smaller the steeper the central density gradient (higher γ). For fixed central flattening (p_0, q_0) ϵ_R is a function of the intrinsic axis ratio. $\epsilon_R = 0.4$ is the upper limit beyond which the epicyclic approximation is no longer valid and the description of the gas on closed orbits breaks down (see Fig. 1 of ZC).

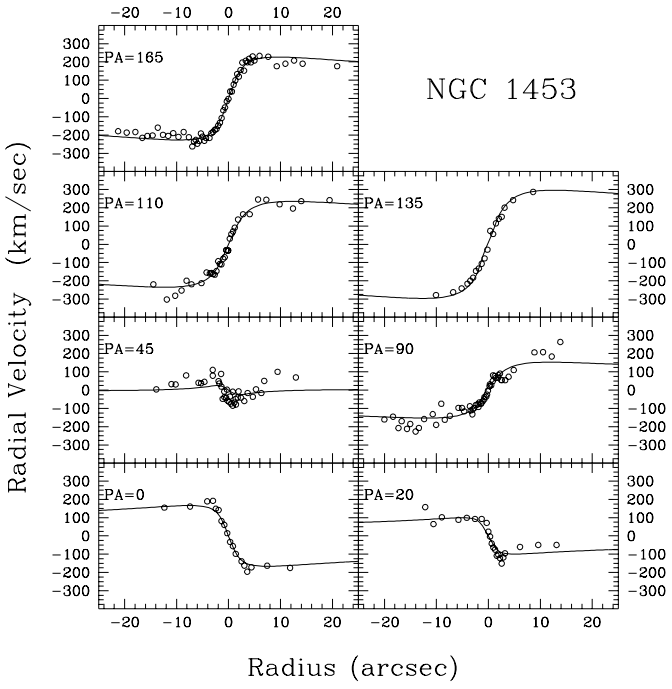

Fig. 1. Observed (open dots) and model (full line) radial velocities curves for NGC 1453.

3. The modelling

3.1. Mass density profile

The method used by B91 to obtain a local M/L_B profile for NGC 5077 consisted of two distinct steps: the determination of viewing angles and intrinsic axial ratios from the observed mean values for the ellipticity and position angle of the stellar component and the observed range for the inclination angle θ allowed by the apparent axis ratio of the gas component. For each of the two possible configurations (gas disk perpendicular to the short axis or perpendicular to the long axis), B91 fit the gas velocity field and obtained a set of parameters related to the total mass, to the core radius and to the asymptotic behaviour of the velocity curves respectively. The derived values then fix the intrinsic density profile. In this paper our aim is essentially the same, determining the intrinsic shape of the ellipsoid and then fitting the observed velocity field.

To model the observed velocity field it is necessary to know the intrinsic axial ratios of the density distribution and the viewing angles. There is not a unique way to deproject the image of a triaxial galaxy projected on the sky since there are more unknown quantities than observables. The γ-models allow us to correlate p_0,q_0,p_∞,q_∞,θ,ϕ,χ and γ to the observed ellipticity and position angles of the stellar major axis at small and large radii (ϵ_0,ϵ_∞,$\Psi_{*,0}$,$\Psi_{*,\infty}$). Hence four quantities out of eight are free to cover the entire range of values in which they are defined. We will determine the value of these four parameters from the velocity field fit. We now discuss the procedure step by step.

The first step consists of finding the proper center and systemic velocity for all the velocity curves. This is done by fit-

ting a simple (circular) velocity field to the data. The next step is to find all the possible combinations of the parameters, $p_0, q_0, p_\infty, q_\infty, \theta, \phi, \chi$ and γ that reproduce the observed shape of the galaxy.

We thus calculate $p_0, q_0, p_\infty, q_\infty$ on a 4-dimensional grid obtained varying the three viewing angles and γ with $0° < \theta \leq 90°$, $-90° \leq \phi \leq 90°$, $0 < \gamma < 2$. χ is chosen to be within a reasonably range around the apparent minor axis of the gaseous disk. Among all the possible combinations of the above parameters, some lead to non–physical models because ϵ_R, the orbital ellipticity in the center, becomes greater than 0.4 and/or the mass density along the short axis becomes negative for some values of the radius r. We then selected the sets of parameters that matches the two above criteria. At this point, for each set of the parameters so far obtained, the best fit model has been derived by means of a least squares fit to the observed velocity field. That is, for each set of parameters (p_0, q_0, p_∞, q_∞, θ, ϕ, χ, γ) that reproduce the observed ($\epsilon_0, \epsilon_\infty, \Psi_{*,0}, \Psi_{*,\infty}$) and that are physically allowable we found the value for r_0 and $\mathscr{M}_\mathscr{T}$ that best reproduced the observed velocity field minimizing the root–mean–square. The set of parameters that, among all, give the minimum r.m.s. represents the best fit of the velocity field.

Because the selected sets of parameters are usually very large, this procedure is iterated using smaller and smaller steps for θ, ϕ, χ and γ around the best fitting parameter-set, as mentioned above. The model velocities are convolved for the seeing before the comparison with the observed values. A gaussian PSF has been used.

An extra constraint on θ can by found from the morphology of the ionized gas. Since the gas orbits become nearly circular at large radii, the apparent axis ratio of the gas disk is directly related to the inclination angle θ. Assuming the disk intrinsically circular, the observed axis ratio is equal to $\cos\theta$. We do not use this constraint because we don't know how the emissivity of the gas varies with position and we do not know whether the disk is flat and circular or thick, warped and elliptical. We thus consider this value of θ as only a rough check for our determination.

3.2. Light density profile

To derive the luminosity density of a galaxy we have to fit the surface brightness profile μ_B taking into account the triaxial shape of the galaxy. Using the value of the three viewing angles previously determined by means of the kinematical fit, we fit the surface brightness profile using the constraints imposed by the twisting of the isophotes and the variation in the ellipticity profile of the stellar component as we did in the previous section. The γ model gives an explicit analytical form for the projected surface density:

$$\Sigma(R, \Psi) = \Sigma_0(R) + \Sigma_2(R) \cos 2(\Psi - \Psi_*) \quad (2)$$

where Ψ_* is the position angle of the stellar major axis, (R, Ψ) is again the generic point of the galaxy projected on the plane of the sky and Σ_0 is the azimuthally averaged surface density profile. Expression can be found in ZC. The fit to the observed surface brightness profile involves, as usual, ten parameters, $p_0, q_0, p_\infty, q_\infty, \theta, \phi, \chi$, γ, r_0 and L_T. The three viewing angles θ, ϕ and χ are now fixed to the values given by the mass density model. Because $p_0, q_0, p_\infty, q_\infty$ depend not only on $\epsilon_0, \epsilon_\infty, \Psi_{*,0}, \Psi_{*,\infty}$ but also on γ, it is possible for their values to be different from the values found in the kinematical fit. This fitting procedure allows one to fit the surface brightness profile and at the same time to roughly reproduce the observed ellipticity and position angle radial profile.

Table 1. The objects. Columns 2-5 are taken from RC3.

Object	Type	B_T^0	R_e	Dist.	L_{TB}	scale
			"	Mpc	$10^{10} L_{B\odot}$	pc/"
NGC 1453	E2	12.2	24.9	77	12.7	374
NGC 2974	E4	11.8	24.3	39	4.3	188
NGC 5077	E3	12.2	22.7	56	6.4	271
NGC 7097	E5	12.6	18.1	45	3.8	220

3.3. Statistical errors in the velocity field modeling

We have not derived in a rigorous way the statistical uncertainties of the parameters obtained for the dynamical model. To this aim we would need the standard deviation of each velocity measurement while only an estimate of it is available. (Paper II). For this reason we cannot obtain the χ^2 of our models. Nevertheless it is important to have an estimate of how much each parameter is constrained by the fit. Using the value σ_{vel} = 15 km/s as the standard deviation of all the velocity measurements, for each best fitting set of parameters (γ, r_0, $\mathscr{M}_\mathscr{T}$, θ, ϕ, χ) we computed the 68% confidence region. We did not include the axial ratios p_0, q_0, p_∞, q_∞ in the above parameter list because the error on this four quantities depends mostly on the error in the measured ϵ_0, ϵ_∞. The error estimate of the model parameters is given only in the cases of NGC 1453 and NGC 2974.

4. The objects

Out of the six galaxies observed in Paper II, only 3 are suitable for a detailed model study of the velocity field, namely NGC 1453, NGC 2974, NGC 7097. In the other 3 galaxies the presence of more than one kinematical component (NGC 3962, NGC 6868) or the non regularity of the gas velocity field (NGC 4636) invalidate the analysis that we are considering in the present paper. We apply the triaxial model also to NGC 5077 previously studied by B91. For the first three galaxies we adopted the same distances as Paper I while for NGC 5077 we considered the same distance adopted by B91. We assumed H_0 = 50 km/s/Mpc throughout this paper. The sample objects are listed in Table 1.

4.1. NGC 1453

NGC 1453 is an E2 galaxy with B_T^0 = 12.21, R_e = 24.9″ (RC3) and a distance of 77 Mpc . The H_α image (Paper I) reveals the presence of an ionized gas disk misaligned with respect to the stellar isophotes by $\sim 56°$. This misalignment together with the

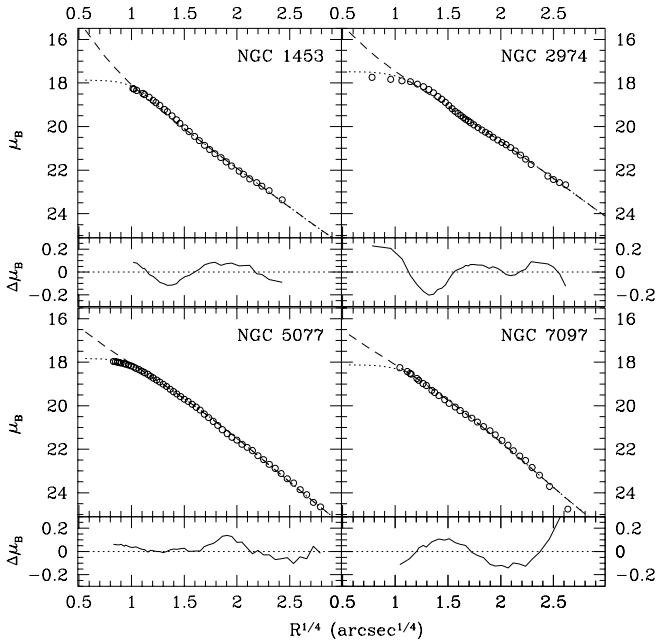

Fig. 2. Modeling the surface brightness profile of the four galaxies studied. In the upper panels the observed (open dots) and model surface brightness profile along the major axis of the objects are plotted. The dashed and dotted lines represents the model profile before and after the seeing convolution respectively. In the lower panels the full line represents the residuals $\Delta\mu = (\mu_{observed} - \mu_{convolved\,model})$.

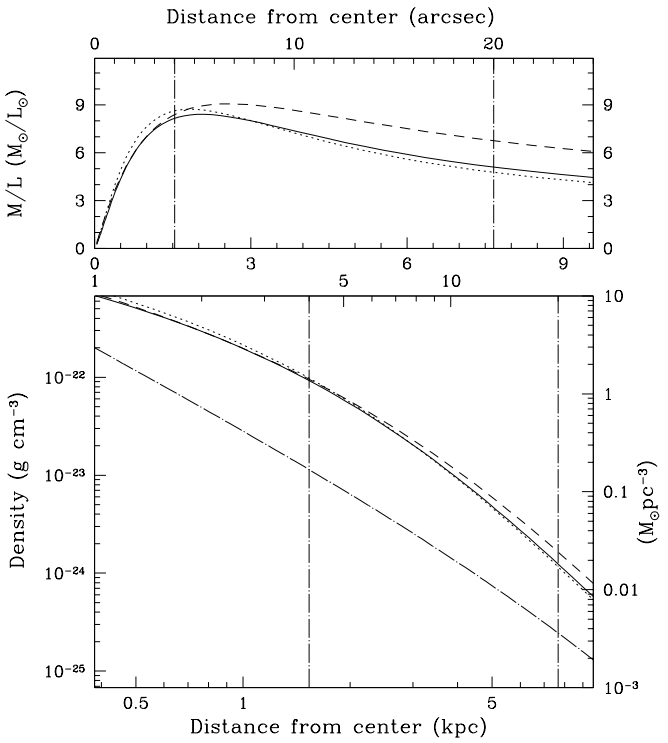

Fig. 3. NGC 1453. Lower panel: mass and light (long dashed line) density profiles for the triaxial model listed in Table 2; the different lines represents the best fit kinematical model (full line) and the two models with the highest and lowest M/L values at large r at the edge of the 68% confidence region (dotted and dashed lines). The radial distance is measured along the intermediate axis. Upper panel: local M/L_B ratio given by the ratio of the profiles of the lower panel. The vertical lines in both the lower and upper panels define the spatial region within which the M/L profile is valid. The inner limit is due to the seeing while the outer limit represents the outermost last available kinematical measurement.

10° twisting of the isophotes suggests that the intrinsic shape of NGC 1453 is triaxial. We have considered the geometrical constraints deduced in paper I $\epsilon_0 = 0.14, \epsilon_\infty = 0.18, \Psi_0 = 27°, \Psi_\infty = 37°$. Using this set of values we determined all the possible intrinsic shapes varying γ, θ, ϕ and χ, and then we fitted the velocity field as described in Sect. 3. The best fit model is listed in Table 2. In Fig. 1 we plot the observed and the best fit velocity field. The mass, luminosity and M/L profiles of the models are shown in Fig. 3. For the modeling of the surface brightness we used the blue profile of Sparks et al. (1991) with a $FWHM$ of the seeing of 2.2″. The result of the photometric fit is plotted in Fig. 2, is listed in Table 2 and the corresponding density profile is plotted in Fig. 3.

The model is able to reproduce the observed velocity field in a satisfactory way. Even along the minor axis (PA 45°), where a spherical model will give zero velocity, the triaxial model shows good agreement with the observational data. The result of our analysis is the following: the gaseous disk is ⊥ the major axis; the galaxy is oriented with viewing angles $\theta = 46° \pm 7°$, $\phi = 54° \pm 8°$ and $\chi = 45° \pm 1°$; the intrinsic axial ratios are $I/L|_0 = 0.86$, $m/L|_0 = 0.75$, $I/L|_\infty = 0.78$, $m/L|_\infty = 0.69$. The mass-to-light ratio radial profile slightly decreases from the value of $\sim 8 M_\odot/L_{B\odot}$ at the innermost point to $\sim 6 M_\odot/L_{B\odot}$ at the outermost point.

4.2. NGC 2974

NGC 2974 is an E4 of $B_T^0 = 11.8$ and $R_e = 24.3''$ (RC3) and 38.8 Mpc distant. The H_α image (Paper I) shows the presence of an ionized gas disk misaligned with respect to the stellar isophotes by about 20°. The velocity field of the gas has been observed with 10 spectra taken at 8 different position angles. Three of these spectra have low spatial and wavelength resolution with respect to the others. For this reason we only considered, for our kinematical modeling, the spectra at PA 45° which add a new position angle to the 7 observed with higher resolution. NGC 2974 also possesses an HI disk which extends out to $3.3 R_e$ (Kim et al. 1988). The HI disk has the same rotation axis and velocity as the inner ionized one. It is likely that the two disks are actually the same structure.

In the application of the triaxial model we assumed the following geometrical constraints: $\epsilon_0 = \epsilon_\infty = 0.34$, $\Psi_0 = \Psi_\infty = 40°$ taking into account that a faint stellar disk is present in this galaxy (Cinzano & van der Marel 1994). The results of our kinematical fit are listed in Table 2 and plotted in Fig. 4. For the

Table 2. Triaxial models: best fit parameters. Parameter sets for different fits of the velocity field and of the surface brightness profile. (1) object; (2) FWHM (arcsec) of the seeing; (3) γ; (4) scale length r_0 (arcsec); (5) total mass $\mathscr{M}_{\mathscr{T}}$ (in units of $10^{11} M_\odot$ for the velocity field fit) or total blue luminosity L_T (in units of $10^{10} L_\odot$ for the surface brightness fit); (6) (7) viewing angles θ,ϕ and χ (degrees); (8)-(11) axial ratios; (12) r.m.s of the fit in units of km/s and $\mu/''^2$ for the velocity field and surface brightness fits respectively. For NGC 1453 and NGC 2974 also the 68% confidence region is reported.

object	seeing	γ	r_0	$\mathscr{M}_{\mathscr{T}}$-$L_T$	θ,ϕ	χ	p_0	q_0	p_∞	q_∞	r.m.s.
(1)	(2)	(3)	(4)	(5)	(6)	(7)	(8)	(9)	(10)	(11)	(12)
Velocity field fit											
NGC 1453	2.3	$0.62^{+0.21}_{-0.05}$	$7.0^{+1.8}_{-0.6}$	$5.06^{+0.73}_{-0.20}$	46^{+6}_{-8},54^{+4}_{-12}	45±1	0.86	1.26	0.84	1.33	$32.06^{+0.14}$
NGC 2974	2.3	$1.14^{+0.29}_{-0.03}$	$11.7^{+6.8}_{-0.6}$	$1.77^{+0.37}_{-0.06}$	57±2,-67±2	139±1	0.76	0.62	0.79	0.53	$26.60^{+0.08}$
NGC 5077	2.3	1.12	18.7	4.32	43,-43	-3	0.77	1.74	0.75	1.29	33.9
NGC 7097	1.5	1.82	433	146	60,29	67	0.61	0.56	0.51	0.49	30.6
Surface brightness fit											
NGC 1453	2.2	1.95	40.2	10.6	46,54	45	0.84	1.22	0.85	1.33	$6.9\,10^{-2}$
NGC 2974	2.2	1.63	29.6	6.13	53,-69	138	0.80	0.58	0.83	0.30	$9.8\,10^{-2}$
NGC 5077	1.5	1.42	17.9	5.60	43,-43	-3	0.75	1.68	0.75	1.29	$6.4\,10^{-2}$
NGC 7097	2.2	1.33	13.8	3.79	60,29	67	0.60	0.55	0.39	0.39	$1.1\,10^{-1}$

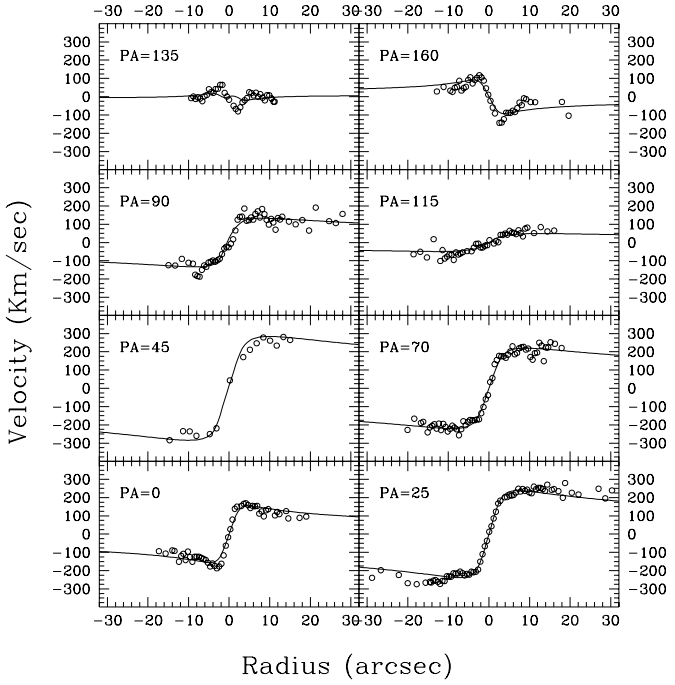

Fig. 4. Observed (open dots) and model (full line) radial velocities curves for NGC 2974.

luminous density model we used the surface brightness profile by Djorgovski (1985) assuming a FWHM of the seeing of $2.2''$. Since this profile is in the R band we transformed it to the B band by adding the $B-R$ color of the galaxy, which equals 1.66 (Poulain & Nieto 1994). The result of the luminosity fit is plotted in Fig. 2 and listed in Table 2.

The corresponding mass, luminosity and M/L profiles are plotted in Fig. 5. The value of the inclination angle θ is well constrained by the model to be $\theta = 57° \pm 2°$ while $\phi = 67° \pm 2°$ and $\chi = 139° \pm 1°$. The intrinsic shape of the galaxy is triaxial with axial ratios $I/L|_0 = 0.76$, $m/L|_0 = 0.62$, $I/L|_\infty = 0.79$, $m/L|_\infty = 0.52$ with the gas moving on the principal plane $\perp$ the short axis. The M/L radial profile decreases from $\sim 4 M_\odot/L_{B\odot}$ at the innermost point to ~ 2.5 at the outermost point. This value is smaller than the value of $5 M_\odot/L_{B\odot}$ obtained by Cinzano & van der Marel (1994) studying the stellar dynamics.

4.3. NGC 5077

NGC 5077, an E3 galaxy with a prominent minor axis dust lane, has been the subject of a detailed study by B91 who modelled its ionized gas velocity field by means of a triaxial potential without a cusp. We assumed $\epsilon_0 = 0.28$, $\epsilon_\infty = 0.20$, $\Psi_{*,0} = 8°$, $\Psi_{*,\infty} = 10°$ (from B91) finding that the gaseous disk lies in the plane $\perp$ to the long axis. This is as expected, because the ionized gas lies almost perpendicular to the apparent major axis. No solutions are found for a gaseous disk laying in the plane $\perp$ to the short axis.

The best fitting values for NGC 5077 are shown in Table 2 and the model velocity curves are plotted in Fig. 6. The angle χ is well determined by the fit and lies close to PA= $-3°$, The viewing angle θ is poorly determined by the fit and, as a consequence, it gives an uncertainty in the determination of the total mass of the galaxy but it does not influence the trend of the density profile. The value of $\theta = 43°$ found in this paper is close to the lower limit stated by B91. The result of the luminosity fit is plotted in Fig. 2 and listed in Table 2. The light and mass density profiles as well as the local M/L_B ratio profile are plotted in Fig. 7.

The results obtained in the present work are in reasonable agreement with B91. Due to the more restrictive geometrical constraints here considered, i.e., not only the twisting between the stellar body and the gaseous disk but also the twisting between the inner and outer stellar isophotes, we do not find solutions for the gas occupying the plane perpendicular to the short

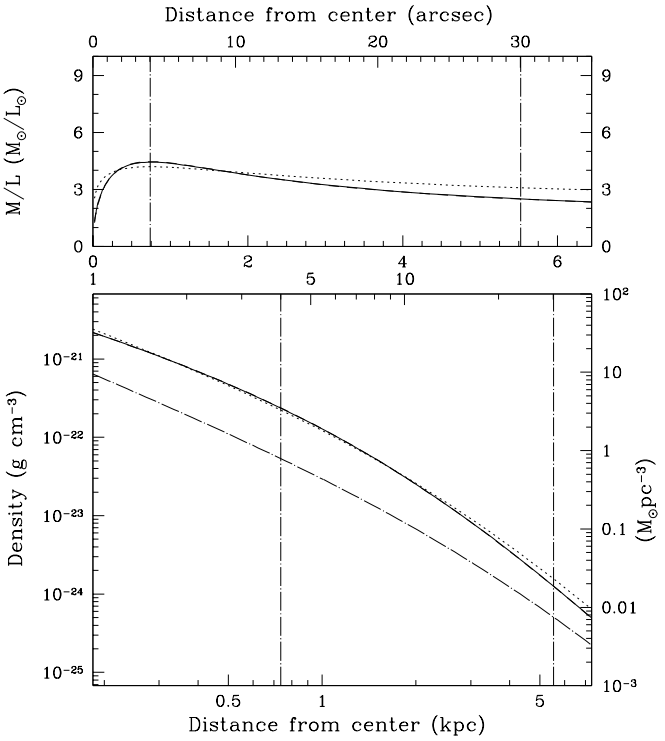

Fig. 5. As Fig. 3 for NGC 2974. The 68% confidence region is bounded by the highest M/L model (dotted line) and by the best model (full line) that, in this case, represents also the lowest M/L model.

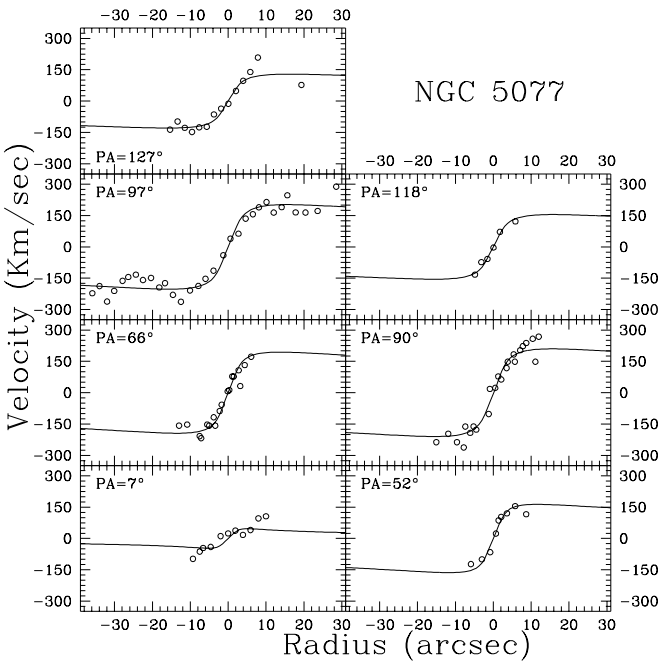

Fig. 6. Observed (open dots) and model (full line) radial velocities curves for NGC 5077.

axis. The viewing angles that we find ($\theta = 43°, \phi = -43°$) fall in the range indicated by B91. The axial ratios ($I/L|_0 = 0.59$, $m/L|_0 = 0.45$, $I/L|_\infty = 0.77$, $m/L|_\infty = 0.58$ also are in the region indicated by B91. The M/L profile increases slowly from the value of $4M_\odot/L_{B\odot}$ in the center to $8M_\odot/L_{B\odot}$ at the last measured point. This result is also consistent with B91, the higher value of M/L being due to the lower value of θ here considered.

4.4. NGC 7097

NGC 7097 is an E5 of $B_T^0 = 12.6$, $R_e = 18.1''$ (RC3) at a distance of 45 Mpc. The stellar kinematics reveal a counterrotating core (Caldwell et al. 1986, Pizzella et al. 1996). The ionized gas velocity field of NGC 7097 has been studied by Caldwell et al. (1986). They considered a gaseous disk inclined at $\theta = 60°$ with respect to the line of sight finding an M/L ratio varying from less than $1''$ in the center to $3.5M_\odot/L_{B\odot}$ at the last measured point, at $12''$.

For this galaxy we have 5 spectra at different position angles. The H_α image (Paper I) shows the presence of an ionized gas disk misaligned by about 30° with respect to the stellar isophotes and with an inclination of 57°. The geometrical constraints considered are $\epsilon_0 = 0.2, \epsilon_\infty = 0.26, \Psi_0 = 15°, \Psi_\infty = 20°$ as indicated by the ϵ and PA profiles in Paper I. When we apply the triaxial modeling we find a low value of the inclination, less than 10°. This result is in contradiction with the indication of the H_α image. Moreover the projected rotation velocity is about $200\,km/s$ (Fig. 8) and a face-on disk will produce huge and unusual deprojected rotation velocities. The problem is mainly due to the rotation curve of PA 90° as is clearly visible in Fig. 8 which represents the best fit kinematical model. The poor fitting of this curve is not an artifact of the triaxial modeling. Neither an error of the position angle of the slit during the exposure can justify the discrepancy between the observation and the model velocity curves. After these considerations, we decided to use the value of θ indicated by the H_α image ($\theta = 60°$) and proceeded with the modeling. For the luminous density model we used the surface brightness profile by Sparks et al. (1991) plotted in Fig. 2 together with the best fit luminous model. In Table 2 we report the results of the kinematical and luminosity models while in Fig. 9 we show the mass and luminous density profile with the M/L profile. The geometrical constraints indicate that the gas is moving in the plane perpendicular to the short axis. M/L is constant with radius and is $8M_\odot/L_{B\odot}$.

5. Discussion and conclusion

We have modelled the gravitational potential of 4 elliptical galaxies using a triaxial mass distribution. The models are able to reproduce the observed velocity fields in a satisfactory way. In particular, in the case of NGC 1453 the model reproduces the non-circular motion along the minor axis of the gaseous disk (PA 45°) at least in a qualitative way. Also in the case of NGC 2974 there is evidence of non zero velocities along the minor axis (PA 135°) but in this case our model is not able to reproduce this effect.

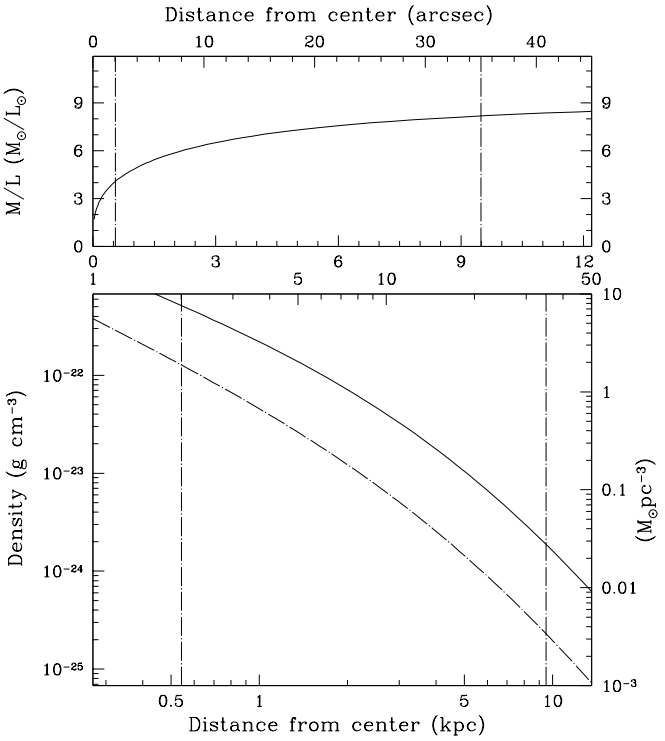

Fig. 7. As Fig. 3 for NGC 5077. Only the best fit model is plotted.

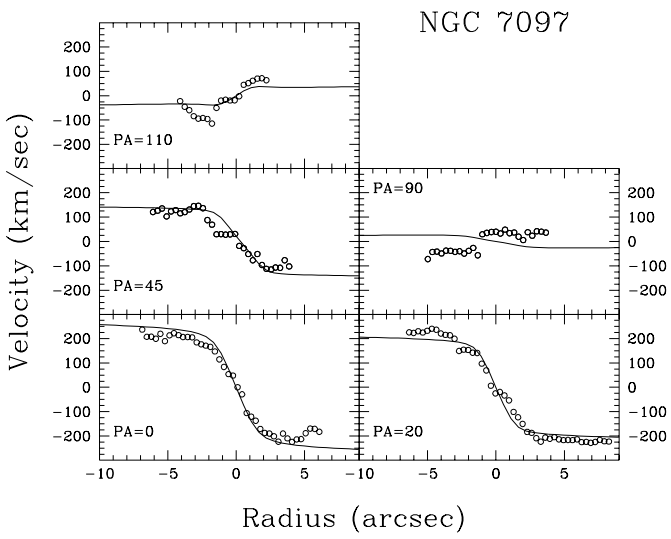

Fig. 8. Observed (open dots) and model (full line) radial velocities curves for NGC 7097.

For NGC 5077 we find good agreement between the model and the observations. NGC 7097 is the only galaxy for which the model was not been able to reproduce the observed gas kinematics. The discrepancy occurs mostly at a single position angle. We remark that the improvement given by the triaxial modeling is not only in reproducing the velocity field, but also the two dimensional shape and the viewing angles of the galaxy. The present method gives also a result that is not strongly model dependent. The only important assumption is that the gas has settled in the principal plane and that it is moving in ordered orbits.

In 2 out of 4 objects (NGC 2974 and NGC 7097), the gas is moving in the plane $\perp$ to the short axis while in the other two cases (NGC 1453 and NGC 5077) the gas is on a plane $\perp$ to the major axis as expected if the gas has an external origin. The resulting M/L profiles are nearly constant with radius. It has to be noted that, even if the model has been convolved for the seeing, both the mass and the light density distribution (and M/L profile) are not reliable in the inner arcsecs. From simple numerical simulation we estimate the limit of $r \sim 4''$ to be the limit inside which the derived M/L profile can be disturbed by the seeing. Moreover the ionized gas velocity fields of the sample galaxies have a central peak in the velocity dispersion. In the inner $4''$ the velocity dispersion that for NGC 2974 reaches the value of $250\,km/s$. This high value can be attributed only partially to an effect induced by the seeing. Indeed, when the central velocity gradient is high, the seeing blurs the spectra lowering the central velocity gradient and increasing the value of the velocity dispersion. By means of numerical simulations we found that, for NGC 2974, the seeing could produce a value of the velocity dispersion not higher than $150\,km/s$ and hence cannot account for the observed value of $250\,km/s$. It is possible that in this central region the ionized gas can be supported by pressure (Bertola et al. 1995, van der Bosch & van der Marel 1995).

The largest radial variation of our derived M/L profiles is an increase by a factor of 2 from the center to the outer regions of NGC 5077. For the other 3 galaxies we observe a constant value (in NGC 7097) and a decrease by a factor of 1.6 and 1.3 (in NGC 2974 and NGC 1453 respectively). The fact that when all galaxies are averaged we do not observe an overall trend (*i.e.* a systematic increase of M/L as we expect if dark matter is present) indicates that luminous matter dominates the mass distribution inside $1R_e$. M/L seems to be higher for objects of higher luminosity and the mean value of M/L is about $5M_\odot/L_{B\odot}$. This value matches well the mean value of $M/L \sim 5$ found by van der Marel (1991) for galaxies of the same mean luminosity. Previous dynamical studies of the ESO Key Programme (Saglia et al. 1993; Bertin et al. 1994) also are consistent with the present indication that M/L is approximatively constant out to $1R_e$ at a value of about $5M_\odot/L_{B\odot}$. We found the presence of dark matter in 3 out of the 9 objects of the sample whose kinematics was measured typically out to 1-2R_e. We can consider this as an indication that the central regions of elliptical galaxies are dominated by the luminous matter while dark matter begins to be dynamically important at 2-3R_e. Only beyond this limit the presence of dark matter is compelling (Bertola et al. 1993; Carollo et al. 1995).

The use of ionized gas kinematics described in the present work provides a good determination of the mass-to-light ratio in the inner regions of elliptical galaxies (inside $1R_e$), where it turns out to show only little variations. It is encouraging to note that our analysis, based on a method which is completely inde-

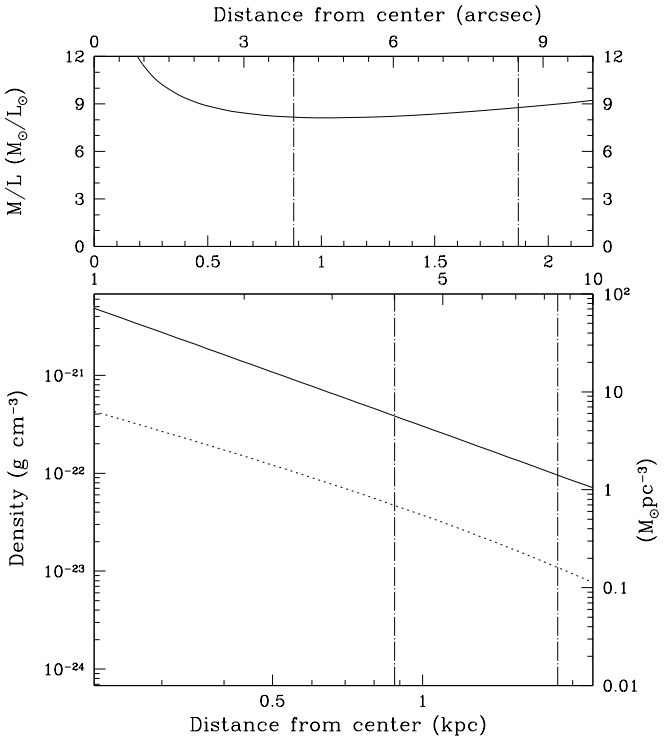

Fig. 9. As Fig. 3 for NGC 7097. Only the best fit model is plotted.

pendent from the use of the stellar kinematics, leads to results that are in good agreement with those obtained with the most recent stellar dynamical models.

To detect the presence of dark matter it is therefore necessary to determine M/L at distances well beyond $1\,R_e$ from the center. In the framework of the present Key Programme this means to use more extended gaseous disks, such as the HI disks which sometimes are observed in elliptical galaxies. As far as the use of the stellar dynamics is concerned, an improvement can be obtained by observing the line profiles at the farthest distances allowed by the state of the art detectors. The determination of the velocity dispersion together with that of the shape of the lines allows one to obtain results which are not model dependent. These results could be compared with those, which are now in a way of rapid accumulation, based on the X-ray halo emission and on the dynamics of planetary nebula.

Acknowledgements. AP acknowledges support from a *Acciaierie Beltrame* grant. RPS acknowledges the financial support by the Deutsche Forschungsgemeinschaft under SFB 328 and 375. WWZ acknowledges the support of the Hochschuljubliäumsstiftung der Stadt Wien (project H-112/95).

References

Bertin, G., Bertola. F., Buson, L.M., Danziger, J., Dejonghe, H., Sadler, E.M., Saglia, R.P., Vietri, M., de Zeeuw, P.T., Zeilinger, W.W., 1989, The Messanger 56, 19

Bertin, G., Bertola, F., Buson L.M., Danziger, J., Dejonghe, H., Sadler, E.M., Saglia, R.P., de Zeeuw, P.T., Zeilinger, W.W., 1994, A&A 292, 381

Bertola, F., 1987, IAU Symposium 127, Structure,and Dynamics of Elliptical galaxies, ed. P.T. de Zeeuw (Dordrecht: Reidel), p. 135

Bertola, F., Bettoni, D., Danziger, J., Sadler, E., Sparke, L., de Zeeuw, P.T., 1991, AJ 373,369 (B91).

Bertola, F., Pizzella, A., Persic, M., Salucci, P., 1993, ApJ 416, L45

Bertola, F., Cinzano, P., Corsini, E.M., Rix, H., Zeilinger, W.W., 1995, ApJ 448 ,L13

Buson, L., Sadler, E.M., Zeilinger, W.W, Bertin, G., Bertola, F., Danziger, J., Dejonghe, H., Saglia, R.P., de Zeeuw, P.T., 1993, A&A 280, 409 (Paper I).

Caldwell, N., Kirshner, R.P., Richstone, D.O., 1986, ApJ 305, 136

Carollo, C.M., 1993, PhD Thesis, Ludwig Maximilian University, Munich

Carollo, C.M., de Zeeuw, P.T., van der Marel, R.P., Danziger, I.J., Qian, E.E., 1995, ApJ441 L25

Carollo, C.M., Franx, M., Illingworth G.D., Forbes D., 1996, AJ submitted

Cinzano, P., van der Marel, R.P., 1994, MNRAS 270, 325

Crane, P. Stiavelli, M., King, I.R., Deharveng, J.M., Albrecht, R., Barbieri, C., Blades, J.C., Boksenberg, A., Disney, M.J., Jakobsen, P., Kamperman, T.M., Macchetto, F., Mackay, C.D., Paresce, F., Weigelt, G., Baxter, D., Greenfield, P., Jedrzejewski, R., Nota, A., Sparks, W.B., 1993, AJ 106, 1371

Dehnen, W., 1993, MNRAS 265, 250

de Vaucouleurs, G., de Vaucouleurs, A., Corwin, H.G. Jr., Buta. R.J., Paturel, G., & Fouqué, P. 1991, Third Reference Catalog of Bright Galaxies (New York: Springer-Verlag) (RC3)

de Zeeuw, P.T., Carollo, M., 1996, MNRAS 281, 1333 (ZC)

de Zeeuw, P.T. & Franx, M., 1989, ApJ 343, 617 (ZF)

Djorgovski, S.B., 1985; Ph.D. Thesis; pag.38

Kim, D.W., Guhathakurta, P., van Gorkom, J.H., Jura, M., Knapp, G.R., 1988, ApJ 330, 684

Jaffe, W., Ford, H.C., O'Connell, R.W., van der Bosch, F.C., Ferrarese, L., 1994, AJ 108, 1567

Merritt, D.R., de Zeeuw, P.T., 1983, ApJ 267, L19

Pizzella, A., Bernardi, M., Bertin, G., Bertola, F.,de Bruyne, V., Buson, L.M., Dejonghe, H., Saglia, R.P., Stiavelli, M., Zeilinger, W.W., 1996, in preparation

Poulain, P., Nieto, J.L., 1994, A&AS 103, 573

Saglia, R.P., Bertin, G., Bertola, F., Danziger, H., Sadler, E.M., Stiavelli, M., de Zeeuw, P.T., Zeilinger, W.W., 1993, ApJ 403, 567

Sparks, W.B., Wall, J.V., Jorden, P.R., Thorne, D.J., van Breda, I., 1991, ApJ Suppl. 76, 471

Tohline, J.E., Simonson, G.F., Caldwell, N., 1982, ApJ 252, 92

Tremaine, S., Richstone, D.O., Byun, Y., Dressler, A., Faber, S.M., Grillmair, C., Kormendy, J., Lauer, T.R., 1994, ApJ 107, 634

van der Bosch, F.C., van der Marel, R.P., 1995, MNRAS 274, 884

van der Marel, R.P., 1991, MNRAS 253, 710

Zeilinger, W.W., Pizzella, A., Amico, P., Bertin, G., Bertola, F., Buson, L.M., Danziger, I.J., Dejonghe, H., Sadler, E.M., Saglia, R.P., de Zeeuw, P.T., 1996, A&A Suppl. 120, 257(Paper II)

This article was processed by the author using Springer-Verlag LaTeX A&A style file *L-AA* version 3.